NJC

ROYAL SOCIETY OF CHEMISTRY

PAPER

View Article Online
View Journal | View Issue

Cite this: *New J. Chem.*, 2022, **46**, 8324

Identifying molecular fluorophore impurities in the synthesis of low-oxygen-content, carbon nanodots derived from pyrene†

Nadeesha L. Kothalawala,‡[a] Sang Won Kim,‡[b] Namhee Kim, ‡[c] Collan J. Henderson,[a] Minsu Seol,[b] Fuqian Yang, [d] Seung-Yeon Kwak,[b] Kyu Young Hwang,[b] Won-Joon Son, [b] Hyeon-Jin Shin,*[b] Hyeonho Choi, *[b] Byeong-Su Kim *[b] and Doo Young Kim *[a]

Received 25th January 2022,
Accepted 1st April 2022

DOI: 10.1039/d2nj00430e

rsc.li/njc

Carbon dots (C-dots) are a promising class of carbonaceous nanomaterials for bioimaging, catalysis, and optoelectronics. However, their applications are disrupted by recent reports that bright molecular fluorophores are co-produced in the synthesis of C-dots, in particular ones prepared through a bottom-up approach (carbon nanodots (CNDs)), commonly derived from citric acid precursors. The presence of highly emissive molecular fluorophore species obscures the true performance of CNDs and severely challenges the development of CNDs. Here we observe that the issue of molecular fluorophore impurity is still problematic for CNDs which are derived from a different type of precursor, polycylic aromatic hydrocarbons (PAHs). In this study, low-oxygen-content CNDs and small molecular fluorophores are co-produced through hydrothermal condensation of nitropyrene. Extensive and systematic characterization following column chromatographic separation and solvent-induced extraction reveals that molecular fluorophores and CNDs are clearly dissimilar in structure and optical properties. This work highlights that rigorous separation and purification steps need to be taken not only for hydrophilic CNDs but also for low-oxygen-content CNDs.

Introduction

Carbon dots (C-dots) are a promising class of carbonaceous nanomaterials with attractive properties such as tunable photoluminescence, catalytic activity, photostability, and low cytotoxicity.[1–3] The low cost of synthesis and abundance of source materials are significant merits of C-dots.[4] Due to these appealing features, C-dots are considered well-suited to optoelectronics,[5,6] energy conversion and storage,[7–9] and biomedical applications.[3,10–12] C-dots are typically synthesized through two methods, top-down synthesis and bottom-up synthesis. In the top-down synthesis, bulk graphitized carbon materials (carbon black, carbon fiber, graphene oxide, or graphene) are cut into nano-sized particles through acidic oxidation, solvothermal methods, microwave, and sonication assisted methods.[13,14] Bottom-up synthesis involves the assembly of nanoscale carbonaceous particles built from small precursor molecules. Throughout this work, C-dots specifically produced through a bottom-up approach will be labeled as carbon nanodots (CNDs)[15] to distinguish them from ones synthesized using a top-down method. A variety of source materials were utilized for the production of CNDs including citric acid, glucose, and polycyclic aromatic hydrocarbons.[16] Since the initial discoveries of tunable photoluminescence (PL), the development of CNDs for light emitting diodes has been actively pursued,[17–19] with the basic strategy of tuning PL properties by either controlling the size and shape of the particles (diameter of the delocalized graphitic core) or creating functional groups on their periphery.[20–28]

In spite of noticeable progress made in the field, the development of C-dots was severely disrupted by recent reports that the synthesis of C-dots, in particular of CNDs through bottom-up methods, likely involves the co-production of brightly emissive molecular fluorophores.[29,30] For example, fluorescent molecular species were formed during hydrothermal synthesis from citric acid.[31–33] Yang *et al.* isolated

[a] *Department of Chemistry, University of Kentucky, Lexington, Kentucky, 40506, USA. E-mail: dooyoung.kim@uky.edu*
[b] *Samsung Advanced Institute of Technology (SAIT), Samsung Electronics Co. Ltd, Suwon, 16678, Republic of Korea. E-mail: hyeonjin.shin@samsung.com, hono.choi@samsung.com, bskim19@yonsei.ac.kr*
[c] *Department of Chemistry, Yonsei University, 50 Yonsei-ro, Seoul 03722, Republic of Korea*
[d] *Materials Program, Department of Chemical and Materials Engineering, University of Kentucky, Lexington, KY, 40506, USA*

† Electronic supplementary information (ESI) available. See DOI: https://doi.org/10.1039/d2nj00430e

‡ These authors contributed equally to this work.

molecular fluorophores using silica column chromatography and identified them as an incomplete condensation product generated during hydrothermal synthesis with citric acid and diethylamine precursors.[32] Shi *et al.* reported the formation of small organic molecular fluorophores during bottom-up synthesis using citric acid and L-cysteine.[33] In these reports, co-produced molecular fluorophore species were distinctive from CNDs in size, structure, morphology, and optical properties.

Unfortunately, little attention has been paid to this issue of molecular fluorophore impurity generated in the synthesis of CNDs until recently, often leading to the misleading interpretation of CND properties. Because of this issue, the origin of bright and tunable PL from CNDs is still disputable. The presence of molecular emitter impurities hinders the further advancement of CNDs. The separation of molecular fluorophore impurities is of utmost importance to identify the source of PL in CNDs. It is generally straightforward to separate molecular fluorophores from CNDs by column chromatography and dialysis,[30] but the separation may be complicated when two parts are linked through covalent bonds.[30] Although several articles reported the formation of molecular fluorophores, investigations were limited to the production of CNDs with a citric acid precursor. This problem was not investigated for other types of precursors, for example, polycyclic aromatic hydrocarbon (PAH) compounds. While CNDs from citric acid, the most common type of precursor molecule, are typically rich in oxygen (30–45% oxygen content) and highly disordered in structure,[34,35] CNDs from PAHs are more ordered with a lower content of oxygen.[28,36]

Herein we report the synthesis of CNDs through the condensation of substituted PAH, 1,3,6-trinitropyrene (TNP). Molecular fluorophores were separated from CNDs by silica column chromatography. The composition and optical properties of each fraction were thoroughly analyzed to identify the molecular fluorophores and CNDs. Molecular fluorophores exhibited much brighter emissions than CNDs. The separation of molecular fluorophores and CNDs was also accomplished by solvent washout. Dissimilar physicochemical properties, morphologies, chemical structures, and optical properties of molecular fluorophores and CNDs were confirmed by dialysis in methanol, PL measurements, thermogravimetric analysis (TGA), X-ray photoelectron spectroscopy (XPS), Fourier transform infra-red spectroscopy (FT-IR), Raman spectroscopy, matrix-assisted laser desorption/ionization time-of-flight (MALDI-TOF) mass spectrometry, transmission electron microscopy (TEM), and X-ray diffraction analysis (XRD). We identified the molecular fluorophores as incomplete condensation products of TNP. The results reported in this work manifest the systematic separation of bright emitting molecular fluorophores from low emitting CNDs through diverse extraction methods.

Experimental

Materials

All chemicals and solvents used for the syntheses were purchased from commercial suppliers and used without further purification. Pyrene (99%), HNO_3 (70%), NaOH (99%), and HCl (35–37%) were purchased from Sigma-Aldrich. PVDF membrane filters were purchased from Merck Millipore.

Synthesis of CNDs

2 g of pyrene was nitrated in HNO_3 (70%, 160 mL) at 80 °C for 12 hours to produce 1,3,6-trinitropyrene (TNP).[28] After cooling to room temperature, the mixture was filtered and neutralized with NaOH. The resultant powder of TNP (6 gram) was dispersed in NaOH (0.2 M, 1 L) solution under ultrasonication for 1 hour. The suspension was transferred into an autoclave, then heated at 300 °C for 10 hours. The product was filtered with a PVDF membrane filter (pore size 200 nm) to remove any insoluble carbon product and HCl (70%) was added to the filtered solution in a dropwise manner. When the medium is made acidic the solubility of CNDs is decreased due to the protonation of acidic functional groups such as carboxylic and phenolic groups. Hence, CNDs start to aggregate and precipitate in the solution which enable the separation of the CNDs through centrifugation. The product was separated from the liquid using a centrifuge at 15 000 rpm for 10 minutes. The obtained CNDs were dried at 75 °C under vacuum overnight.

Column chromatography

The as-obtained CNDs were separated through a Biotage Isolera flash purification system with a column bridge (IntertecTM, size of 60 g). The column cartridge was uniformly packed with silica gel as the stationary phase and equilibrated with 2.5 column volumes of solvent with low polarity. Then, the screw-top cap of the column cartridge was detached and the remaining solvent on silica gel was eliminated. Next, 0.10 g of crude CND sample was loaded on silica gel and prudently added onto the frit inside the column cartridge. The screw-top cap was then re-attached and eluted with a gradient of solvent mixture using dichloromethane (DCM) and methanol (MeOH) using normal phase column chromatography. The percentage of MeOH in the solvent mixture was changed from 0% to 10% (v:v) during the separation.

Dialysis of column fractions

Dialysis was carried out for each column fraction in MeOH using a regenerated cellulose dialysis membrane (1 kDa MWCO) for 24 hours. The dialysate (solution outside a dialysis bag) and the retentate (solution inside a dialysis bag) were separately collected to test the photoluminescence.

Characterization

UV-Vis absorbance measurements of the column fractions in MeOH were carried out using a Thermo-Scientific Evolution 201 UV-visible spectrophotometer. The samples were scanned in the wavelength range of 200–1000 nm with a bandwidth of 1 nm and 0.1 s integration time. Steady-state emission spectra of the column fractions were recorded using a Horiba Scientific Fluoromax Plus-C fluorometer. The measurements were performed at a series of excitation wavelengths using a 2 nm entrance and exit slits with an integration time of 0.1 s. Fluorescence lifetime measurements were carried out using

the time-correlated single-photon counting method. A DeltaHub™ high throughput time-correlated single-photon-counting (TCSPC) controller connected to the Horiba Scientific Fluoromax Plus-C fluorometer was used with a Nano LED as the pulsed excitation source (excitation wavelength 455 ± 10 nm). The lifetimes were recorded at 584 nm, 515 nm, and 532 nm emission wavelengths, 200 ns measurement range, 5 nm band-pass, and a 1 MHz repetition rate. The instrument response factor (IRF) was obtained using Ludox solution. The lifetime decays were fit, and the lifetime calculations were carried out using Decay Analysis (DAS6) software. The decays were fit using single, two and three exponentials to calculate the lifetime. Absolute photoluminescence quantum yield (PLQY) measurements were performed using the integrated sphere connected to the Horiba Scientific Fluoromax Plus-C fluorometer. The excitation wavelength was 480 nm. 0.5 nm slit width and 0.5 s integration time were the parameters for the PLQY measurements and the calculation of the PLQY was performed using the Horiba Scientific FluorEssence™ software. The spectral range was set to cover both the Rayleigh scattering peak of the excitation and the emission peak from the sample. Methanol was used as the blank and the measurement of the blank was carried out under the same conditions and parameters as the sample. Calculation of PLQY was carried out based on the following equation, PLQY = $[(P_B - P_A)/(L_A - L_B)] \times 100\%$. P_A and P_B are the integrated emission intensities of the blank and the sample, respectively. L_A and L_B are the integrated Rayleigh scattering intensities of the blank and the sample, respectively, in the range of excitation.

XPS measurements were carried out using a Thermo Scientific K-alpha X-ray photoelectron spectrometer with a monochromatic Al Kα X-ray source. The analyzed spot size was 400 μm in diameter. Measurements were carried out with the flood gun. Sample preparation was carried out by drop-casting the samples on to a thoroughly cleaned Si wafer. All the survey spectra and the high-resolution spectra were collected with 10 scans. The XPS data analysis was done by deconvoluting the spectra using Thermo Avantage software. Fourier-transform infrared spectroscopy (FT-IR) measurements were conducted using a Nicolet IS50 FT-IR spectrometer with a diamond attenuated total reflectance (ATR) plate. FT-IR spectra were recorded with 4 cm^{-1} resolution and 64 scans. Samples were drop-cast onto the ATR plate and then dried until the solvent evaporates inside a 60 °C oven.

MALDI-TOF mass spectra were recorded on a Bruker UltrafleXtreme spectrometer using 7,7,8,8-tetracyanoquinodimethane (TCNQ) as the matrix. XRD patterns were obtained with a Bruker D8 Discover system using Cu Kα radiation.

TGA was performed with a Q50 (TA instruments) by ramping up the temperature from 30 °C to 800 °C at the rate of 100 C min^{-1} under the flow of N_2 gas. TEM images in bright-field mode were collected using a JEM-F200 transmission electron microscope (JEOL). Sample preparation for TEM was conducted by drop-casting the sample dispersed in dimethylformamide (DMF) on to a carefully cleaned Si wafer.

Raman spectra of column fractions were obtained using a Thermo Scientific DXR micro-Raman spectrometer equipped with a diode-pump Nd:YVO_4 laser. Measurements were carried out at 532 nm excitation and 0.8 mW laser power. The concentrated solutions of the F_Y, F_G, and F_{CND} samples were poured on a thoroughly cleaned Si wafer and dried in an oven (60 °C) to completely remove the solvent. Raman measurements of the crude sample, pyrene and TNP were also performed for comparison.

Results and discussion

The synthetic procedure of pyrene-derived CNDs is summarized in Scheme 1. This scheme also depicts a hypothetical process in which the pyrene precursor is first nitrated into TNP and then fused into the CNDs through hydrothermal

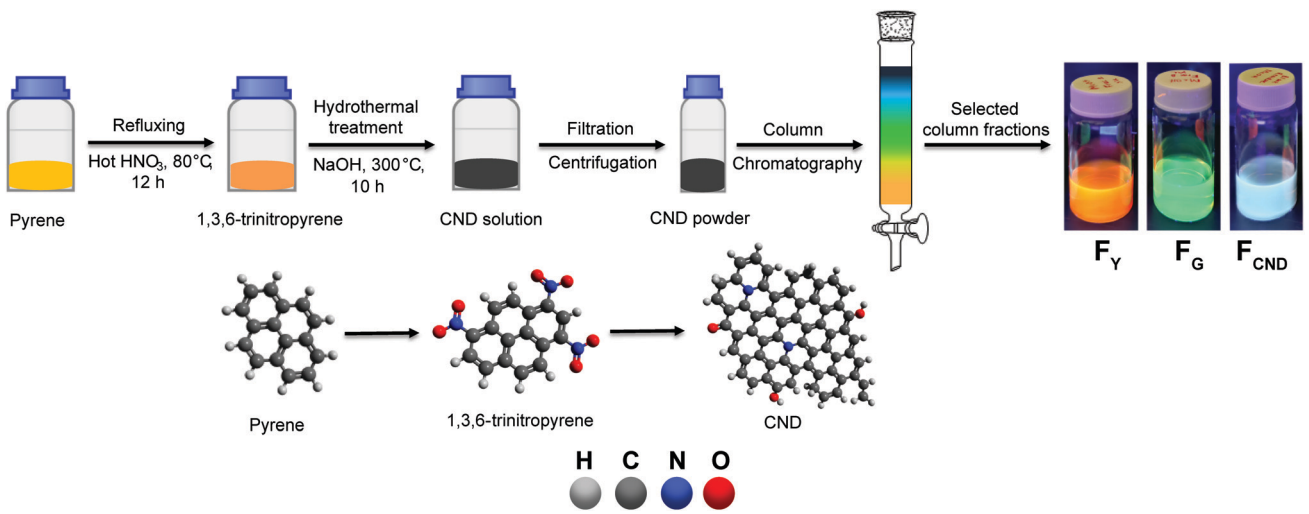

Scheme 1 Procedures to synthesize CNDs and separate fractions through column chromatography. At the bottom, it presents a hypothetical scheme of the synthesis starting from pyrene, to TNP, and to CNDs.

condensation. TNP enhances its reactivity for hydrothermal condensation.[28,37,38] We observed that the fusion of TNP has led to the formation of well-ordered CNDs with good crystallinity (as revealed in the TEM images in the later section), whereas conventional bottom-up pyrolysis of citric acid typically produced highly disordered CNDs.[39,40] Filtration and centrifugation were performed to separate the crude CNDs from the unreacted species. Then, column chromatography was performed to separate the molecular impurities and the CNDs. Several fractions were eluted through a silica column. Among those, three fractions (labeled as F_Y, F_G, and F_{CND}) showing distinctive PL behaviors were further analyzed (Fig. 1).

Fig. 1(a) shows the chromatographic separation of the crude sample under the illumination of UV-light (λ = 365 nm). Among the F_Y, F_G, and F_{CND} fractions, F_Y has the shortest retention time, and it is followed by F_G and F_{CND}. The short retention time of F_Y is attributable to its less polarizable character. As shown in the XPS data in Fig. 2(a) and (b), F_Y contains less sp^2-bonded carbon than F_G. A negatively charged, silica stationary phase of the column can polarize π electrons delocalized in the sp^2-bonded carbon structure, inducing molecular interaction with the stationary phase. The molecular interaction of π electrons with the stationary phase is weaker for F_Y than for F_G, leading to the faster elution of F_Y. The longest retention time of F_{CND} among 3 fractions is attributable to the fact that F_{CND} is significantly larger than F_Y and F_G and has the longest π conjugation through its fully graphitized core. F_Y has yellow emission at 365 nm excitation and F_G gives green emission. F_{CND} appears in the form of a black residue with a bluish-green emission.

The UV-VIS spectra of 3 fractions (F_Y, F_G, and F_{CND}) are shown in Fig. 1(b). The spectrum of F_{CND} is noticeably different from those of F_Y and F_G. F_{CND} exhibits a very broad absorption spectrum in the range of 200 nm to 700 nm with a shoulder at 280 nm due to π–π^* transitions from the sp^2-carbon domain. Broad absorption in the 400–700 nm range represents the transition of surface states present in F_{CND}.[28] This feature of CNDs is commonly reported in the literature.[22] In contrast, F_Y and F_G present relatively sharp bands and vibronic features which are characteristic of molecular fluorophores.[30] The absorption band of F_Y is shifted toward a longer wavelength compared to F_G. This red shift may be due to the structural difference of two molecular species.

Fig. 1(c) presents the time-resolved PL decays of F_Y, F_G and F_{CND} recorded from TCSPC experiments. TCSPC decay parameters for the three fractions are summarized in Table S1

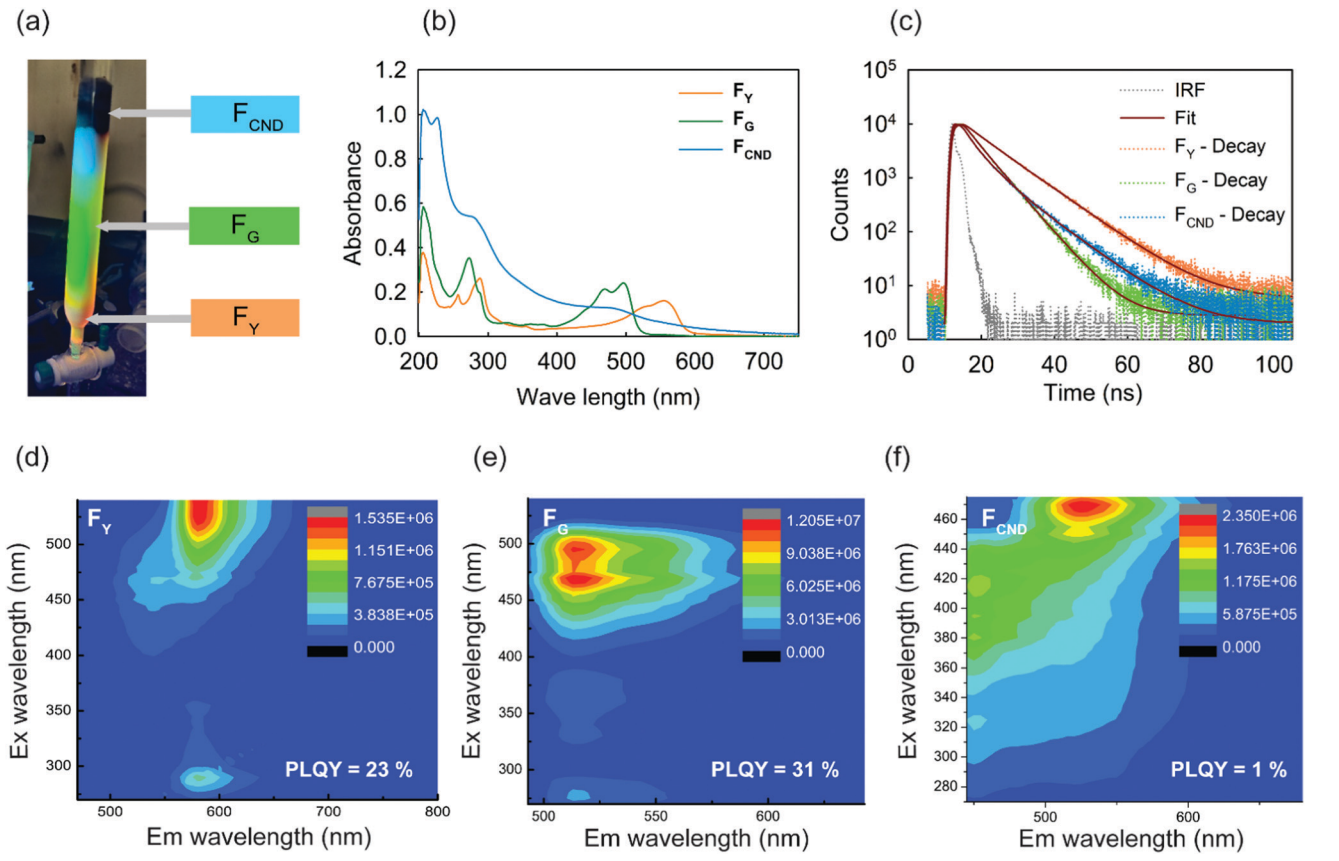

Fig. 1 (a) The photograph of a silica column with the elution of three fractions, F_Y, F_G, and F_{CND}. (b) UV-Vis absorbance spectra of F_Y, F_G, and F_{CND}. (c) PL lifetime decay profiles of F_Y (λ_{Ex} = 455 nm, λ_{Em} = 584 nm) F_G (λ_{Ex} = 455 nm, λ_{Em} = 515 nm) and F_{CND} (λ_{Ex} = 455 nm, λ_{Em} = 532 nm) from time correlated single photon counting (TCSPC) experiments. 3-D PL mapping spectra of (d) F_Y, (e) F_G, and (f) F_{CND} (colored bars in the insets show the PL counts per second).

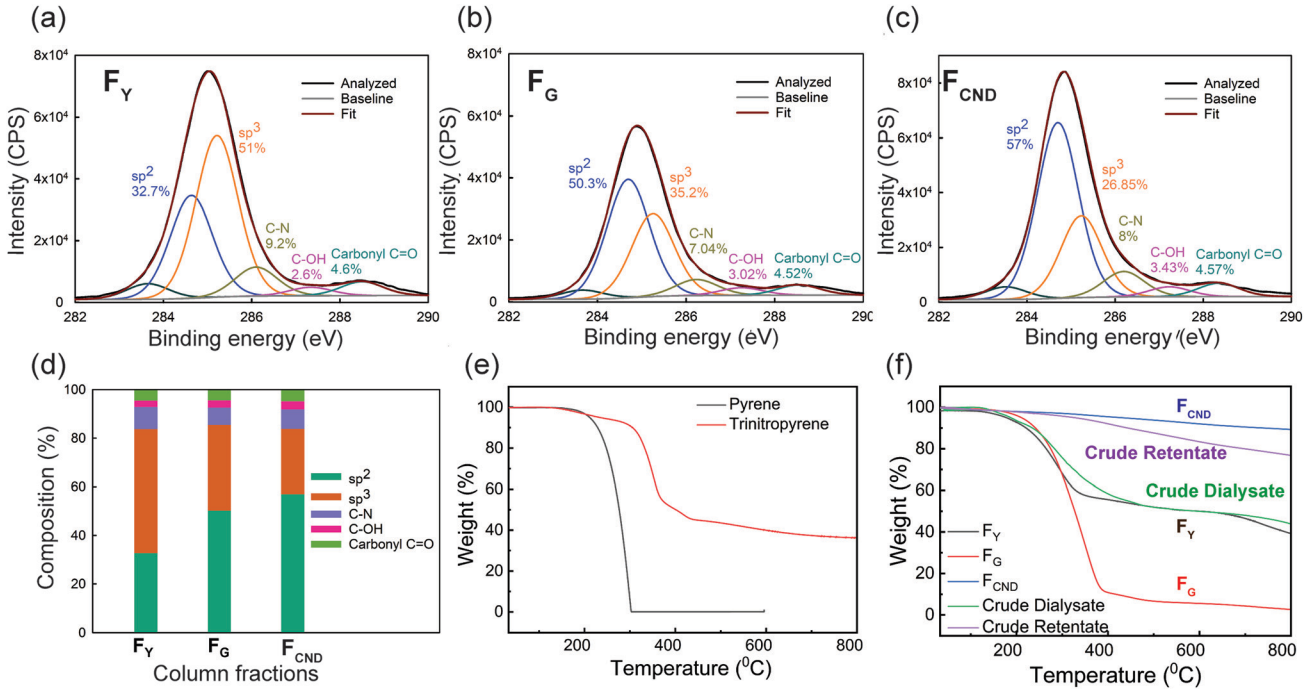

Fig. 2 Deconvoluted high-resolution C 1s XPS spectra of fractions (a) F_Y, (b) F_G, and (c) F_{CND}. (d) Percentages of the chemical states of the carbon element in each fraction determined by XPS analysis, TGA curves of the precursors (e) TNP and pyrene, and (f) F_Y, F_G, F_{CND}, and crude retentate and crude dialysate from dialysis of the crude sample.

(ESI†). PL decay of F_Y fits well with the single exponential decay at 455 nm excitation (τ = 8.9 ns). The 8.9 ns decay is much longer than the intrinsic decay component of CNDs which has been reported in the literature, confirming that F_Y emission is from the molecular fluorophore.[23] F_G shows bi-exponential decay with a fast decay component τ_1 (3.2 ns) and slower decay component τ_2 (5.7 ns). The fast τ_1 component may be from an aggregated form of the molecular fluorophore. In contrast to F_Y and F_G, the decay of F_{CND} fits with three exponentials, representing in the complex and inhomogeneous nature of F_{CND}. Three decay components include a fast decay, τ_1, which corresponds to intrinsic emission from the sp^2-bonded graphitic carbon core of the CNDs and slower decays, τ_2 and τ_3. The τ_2 and τ_3 components are assigned to functional groups on the periphery of the CNDs.[22,30] Notably, the 3 decay components of F_{CND} are in a good agreement with the PL decay of the CNDs reported in the literature which have been synthesized through a top-down method as well as a bottom-up method.[22,23] Based on UV-VIS spectroscopy and TCSPC results, F_Y and F_G can be unarguably assigned to molecular fluorophores and F_{CND} primarily contains CNDs with a larger graphitic core.

Fig. 1(d)–(f) show the 3D PL mapping of three fractions. The PL spectra of F_G and F_Y indicate excitation-independent behavior, indicating the presence of one or only a few chromophores in F_G and F_Y. Conversely, the PL mapping of F_{CND} shows excitation-dependent behavior: the red-shift of emission as the excitation wavelength gets longer. F_G displays green emission with a peak maximum at 515 nm and F_Y shows yellow emission with a peak maximum at 584 nm. The raw emission spectra of the three fractions are given in Fig. S1(d)–(f) (ESI†). The excitation-independent PL of F_Y and F_G along with their higher quantum yields (23% for F_Y and 31% for F_G) is another piece of evidence that F_G and F_Y are molecular fluorophores[30,34] formed during hydrothermal condensation of nitrated pyrene precursors. It is noteworthy that, however, the UV-VIS and PL spectra of F_Y and Y_G are distinguishable from those of pyrene and TNP shown in Fig. S1(a)–(c) (ESI†). The excitation-dependent PL of F_{CND} suggests that this fraction contains multi-chromophoric units and has a heterogeneous structure, in good agreement with the behavior of CNDs commonly reported in the literature. The PL quantum yield of F_{CND} is very low (1%) since the main emitting species in F_{CND} is weakly-emitting CNDs with a large crystalline, graphitic core and low surface oxidation.[30] The photoluminescence excitation (PLE) spectra of F_Y, F_G, and F_{CND} are presented in Fig. S2 (ESI†). The PLE spectra of F_G recorded at two emissions (537 nm, 584 nm) are nearly overlapped, indicating the two emissions come from the same origin. The PLE spectra of F_Y show two bands implying that two emitting species are present. The two emitting species may be ascribed to different types of molecular fluorophores with slight structural and compositional changes. The PLE spectra of F_{CND} recorded at the two main emission wavelengths (455 nm and 540 nm) reveal the possibility of the presence of two emissive species. Based on the TCSPC result of F_{CND} with 3 decay components, F_{CND} may contain molecular fluorophores (or similar structure) covalently bonded to CNDs in addition to the weakly-emitting graphitic core.[30]

Fig. 2(a)–(c) present the high resolution XPS C 1s spectra of F_Y, F_G and F_{CND}. The C 1s high-resolution XPS spectra are

deconvoluted with peaks assigned to sp^2-C (284.6 eV), sp^3-C (285.2 eV), C–N (286.1 eV), hydroxyl C–OH (287.34 eV), and carbonyl C=O (288.5 eV). Bar graphs in Fig. 2(d) summarize the percentages of various chemical states of carbon element in F_Y, F_G, and F_{CND}. Compared to F_G, F_Y possesses a lower sp^2-C content and a higher sp^3-C content, indicating more abundant functional groups. F_{CND} has the highest sp^2-C content and the least sp^3-C content indicating the predominant graphitic domain. In addition to the size of particles in each fraction, their content of sp^2-C may be an important factor to influence the retention behavior as discussed in Fig. 1. Unlike CNDs derived from precursors of citric acid, urea, ethylenediamine, cysteine, and saccharides contain high oxygen contents, we report that PAH-derived CNDs contain a much lower oxygen content (<20%, Fig. S4, ESI†) and a high C/O ratio.

Fig. S3 (ESI†) presents the FT-IR spectra of F_Y, F_G, F_{CND}, and precursor molecules. The FT-IR spectra of F_Y and F_G display sharp peaks in the 700–1600 cm^{-1} range corresponding to C–N stretching, sp^3 C–H bending, and aromatic ring stretching. TNP shows overlapping peaks in the 700–1600 cm^{-1} range indicating their structural similarity. In addition, F_Y and F_G present the peaks for hydroxyl groups (3400 cm^{-1}), amine groups (3250 – 3300 cm^{-1}), and carbonyl groups (1745 cm^{-1}). An aromatic ring stretching (1580 cm^{-1}) is intensified more in FY and FG than in TNP (Fig. S3(e), ESI†), indicating the aromatic ring of the precursor molecule becomes extended during condensation. F_{CND} also displays similar functional groups and content of sp^3-C but presents a marked intensity of aromatic domains (1580 cm^{-1}). Overall, the FT-IR results are consistent with the XPS data, giving a convincing conclusion that F_{CND} is dominated by large sp^2-C graphitic domains whereas F_G and F_Y comprise more confined aromatic domains and functional groups.

TGA provides useful insights about the chemical structure of materials. In Fig. 2(e) and (f), the temperature driven mass loss of materials is recorded for precursor molecules (pyrene and TNP) and three fractions. All TGA experiments were carried out under a N_2 flow.[41] F_Y loses 40% of its weight around 300 °C and remains stable until it is decomposed at 700 °C. This stability of F_Y after 300 °C could be due to the rearrangement of this molecule into a stable structure in the solid form. FG has shown an extensive mass loss (90% loss) at 400 °C. TNP (Fig. 2(e)) shows 50% weight loss at 350 °C indicating that F_Y and TNP may contain similar structures. Pyrene resembles F_G although it is decomposed more rapidly. Unlike other samples, F_{CND} shows negligible mass loss (<10% loss) until 800 °C.[42] Presumably, the large graphitized sp^2 carbon core in F_{CND} makes it very stable against thermal decomposition. TGA analysis was also performed for the dialysate and the retentate of the crude sample (crude sample without any chromatographic separation) as shown in Fig. 2(f). The dialysis of the crude sample was carried out using a 1000 Da molecular weight cut-off (MWCO) membrane for 48 hours. The TGA curve of the dialysate overlaps that of F_Y confirming the presence of the same molecular fluorophores in the crude dialysate. The TGA curve of the retentate shows a trajectory similar to that of F_{CND} indicating that CNDs are the predominant species retained during dialysis. Overall, the TGA results provide strong evidence that small molecular fluorophores were co-produced in the synthesis of CNDs.

Raman spectroscopy is a sensitive tool to probe the microstructure of materials. For example, the D band (1360 cm^{-1}) and G band (1580 cm^{-1}) in the Raman spectrum are the signature of the six-membered, graphitic carbon domains present in the sample. Fig. 3 shows the Raman spectrum of F_{CND} in comparison with those of the F_G, F_Y, crude sample, and the precursor molecules. Some of the samples produce noisy spectra due to the low laser power used in acquiring the signal. This was done to avoid an adverse effect of the Raman excitation laser causing structural damage and pyrolysis through heat accumulation along the surface of less conductive samples. Both the D band and G band are clearly found in F_{CND}. F_G and F_Y show distinct Raman peaks different from each other and F_{CND}. Importantly, the D and G bands are absent in F_Y and F_G suggesting their identity as non-graphitic molecular fluorophores. Some peaks in the spectra of F_Y and F_G closely overlap with those in the spectra of pyrene and TNP (Fig. 3(e) and (f)), implying that molecular fluorophores and precursors share similar structural units. This interpretation is consistent with the outcomes of the TGA results. In the crude sample, the D and G bands are present suggesting the presence of CNDs in the non-purified crude product. Fig. S5 (ESI†) shows the TEM images of F_Y, F_G, and F_{CND}, respectively. While the TEM images of F_Y and F_G show the sparse dark spots in the entire region of the sample, the TEM image of F_{CND} displays dense dark dots with a lateral size of approximately 3–5 nm. Fig. S5(d and e) (ESI†) clearly show graphitic lattice fringes of particles. The spacing of 0.2 nm in the lattice fringes (Fig. S5(e), ESI†) is assigned to the (100) plane of graphite. Taken together, these images provide additional evidence that F_{CND} is primarily composed of graphitic sp^2-bonded carbons unlike F_Y and F_G.

Recent studies urged researchers to perform dialysis as a critical step to separate CNDs from impurities and synthesis

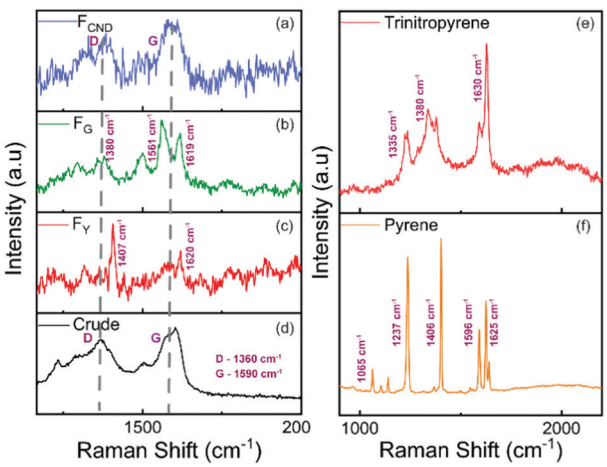

Fig. 3 Raman spectra of the (a) F_{CND}, (b) F_G, (c) F_Y, and (d) crude samples. Raman spectra of (e) TNP and (f) pyrene.

residues. The separation of species through dialysis is based on the difference in size and solvation radii.[28,33,43] It was reported that small molecular fluorophores were successfully separated from the CNDs by dialysis, and a retentate (solution inside a dialysis bag) and a dialysate (solution outside a dialysis bag) were identified as CNDs and molecular fluorophores, respectively.[29,30] It is noteworthy that in most CND dialysis, water is used as the solvent because the CNDs and co-products derived from citric acid are hydrophilic. In contrast, our synthesis using a substituted polyaromatic precursor has produced hydrophobic particles, which are only sparingly soluble in water. The choice of a correct solvent is important to avoid the aggregation of materials which may interrupt the size-driven permeation process across a dialysis membrane. In the current study, the dialysis was carried out for 24 hours in MeOH as the fractions were dissolved in MeOH reasonably well.

The dialysis was performed with F_{CND}, F_Y and F_G, the three fractions which were isolated by column chromatography. Fig. 4(a) illustrates the dialysis procedure and Fig. 4(b)–(g) are the PL spectra of each fraction measured for the retentate part in comparison with the dialysate part. Note that the instrument conditions for the PL experiments (*e.g.*, slit widths, collection time) were kept the same for both retentate and dialysate solutions, and the solution volume of dialysate is 70 times larger than that of the retentate. For F_{CND}, only a negligible PL intensity was observed in the dialysate (Fig. 4(c)) after 24 hours of dialysis indicating that a very small fraction of F_{CND} leaked through the dialysis bag. In contrast, the majority of F_Y and F_G escaped to the dialysate. Based on the volume difference (70 : 1, dialysate: retentate) and the calculation of areas under the PL spectra, 90% of F_G and 99% of F_Y are estimated to leak into the dialysate. Overall, our dialysis results support that F_{CND} particles are significantly larger than F_G and F_Y.

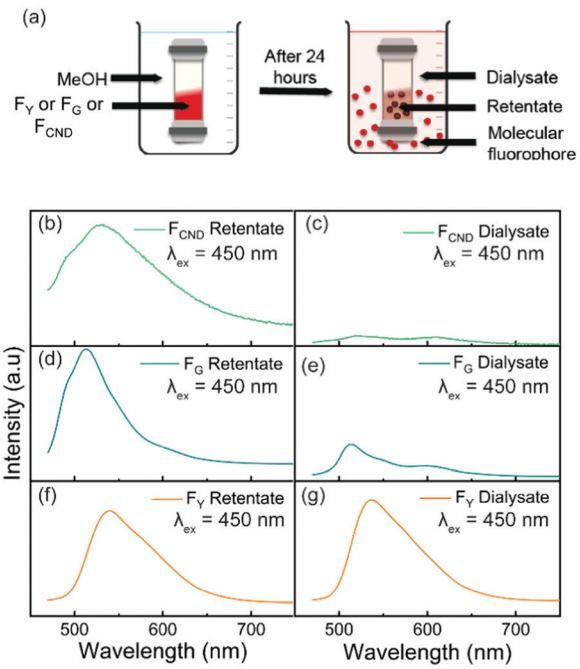

Fig. 4 A schematic illustration of the dialysis procedure. PL spectra of (b) the retentate and (c) the dialysate of F_Y. PL spectra of (d) the retentate and (e) the dialysate of F_G. PL spectra of (f) the retentate and (g) the dialysate of F_{CND}. Note that the PLs of dialysates and retentates were immediately measured after dialysis without concentrating or diluting, and the volume ratio of the dialysate and the retentate in all the fractions is approximately 70 : 1.

Although column chromatography and dialysis successfully separated molecular fluorophores and CNDs, these methods are not applicable for large-quantity samples. Therefore, a simple solvent-based process was tested as a tool, potentially suited to a large-scale production. Acetone and aqueous ammonia solution were used as solvents to extract molecular fluorophores and CNDs, respectively. As shown in Fig. 5, an organic solvent such as acetone is effective in extracting hydrophobic molecular fluorophores. And aqueous ammonia solution (pH 11.2) promotes the dissolution of CNDs by deprotonating hydroxylic groups on the periphery of the CNDs. The detailed procedure of the solvent washouts is illustrated in Fig. S6(a) (ESI†). After extraction with acetone and aqueous ammonia, each washout was passed through vacuum filtration to remove insoluble large particles. Acetone washout solution is denoted as S_A and base washout with aqueous ammonia (pH 11.2) is denoted as S_N. The photographs of S_A and S_N are shown in Fig. S6(b) (ESI†). We attempted to disperse the crude sample in aqueous solution at various pH values; only pH 10.6 and 11.2 solutions successfully dispersed the crude sample (Fig. S6(c), ESI†) indicating the effect of the hydroxylic groups in the sample.

XRD spectra in Fig. 5(a) clearly present the structural difference between S_A and S_N. S_N shows a single, broad peak at 26° which is characteristic of the (002) plane of graphite, implying that graphitic carbon material is the major constituent of this sample. Although the XRD spectrum of S_A also reveals a similar peak around 26°, it presents two additional distinct peaks at 12.1° and 24° that are assigned to the (001) plane and the (002) plane of pyrene derivatives, respectively. These two peaks suggest that S_A contains molecular fluorophores derived from pyrene and TNP. TEM images of S_A and S_N are shown in Fig. 5(b) and (c). In the case of S_A, we didn't observe any atomic symmetry and lattice structure. Instead, needle-like morphology with a length of 100 nm is observed (Fig. 5(b), inset). This needle-like structure was similar to that of pyrene-derivatives reported in the previous publication[44] and may originate from the supramolecular assembly of molecular fluorophores. In contrast, dark circular dots with uniform lateral sizes appear in S_N (Fig. 5(c)) and the high-resolution TEM image of S_N (Fig. 5(c), inset) shows a crystalline structure with a lattice spacing of 0.21 nm corresponding to graphene (100) planes.

To obtain an insight into the chemical structure of S_A and S_N, MALDI-TOF analysis was performed. The resultant mass spectra in Fig. 5(d) show very different distributions of mass-over-charge (m/z) for S_A and S_N. While S_N shows a broad m/z distribution in the 1000–5000 Da range with the maximal intensity around 1500 Da, S_A exhibits a much lower m/z centered around 700 Da. This suggests that particles in S_A are quite small compared with those in S_N. The representative

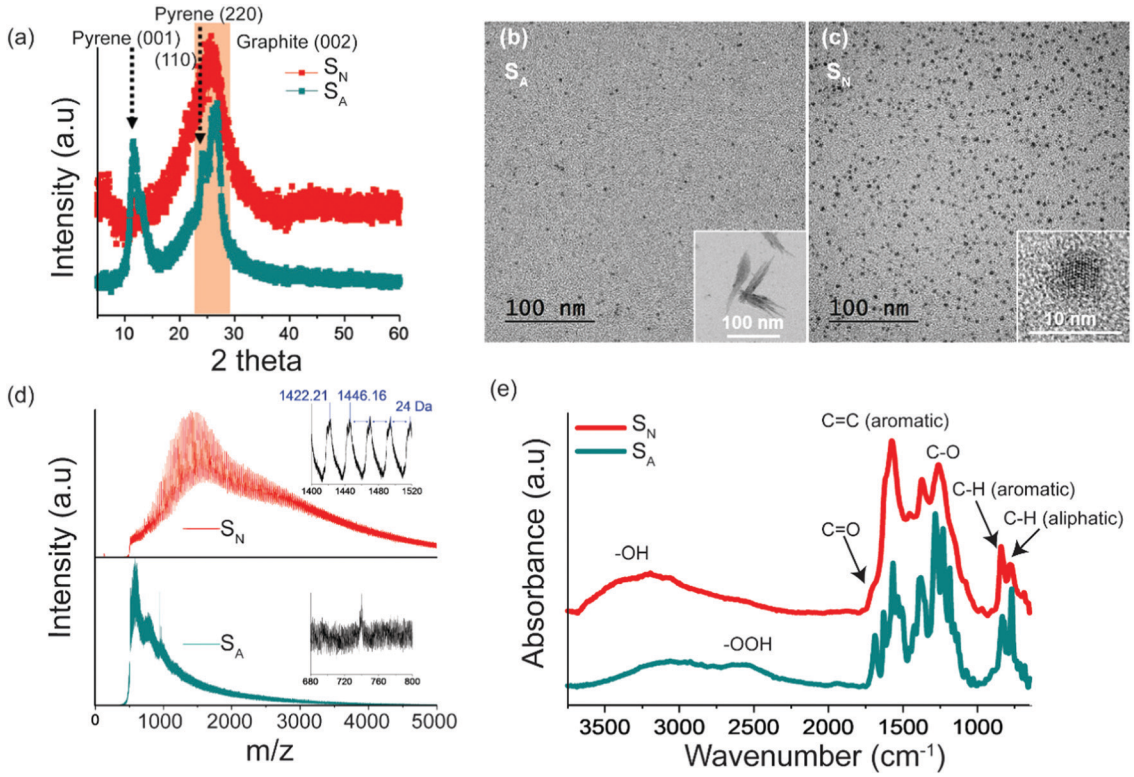

Fig. 5 (a) XRD spectra of S_A and S_N. TEM images of (b) S_A and (c) S_N. Insets in the figures show the high-resolution TEM images of S_A and S_N. (d) MALDI-TOF mass spectra of S_A and S_N. (e) FT-IR spectra of S_A and S_N.

MALDI-TOF signals are depicted in the insets. For S_N, a regular fragmentation pattern with the repeated m/z of 24 is found in the mass spectra, which is interpreted as C=C bonds of polycyclic aromatic carbon compounds.[45,46] For S_A, there is no apparent fragmentation pattern in the whole m/z range. This probably means that the chemical structure of S_A includes not only aromatic units but also aliphatic chains.

FT-IR analysis was performed for S_A and S_N to track their functional groups. In the FT-IR spectra (Fig. 5(e)), both samples show overlapping characteristic peaks related to the –OH stretching vibration at 3000–3500 cm^{-1}, C=O stretching at 1690 cm^{-1}, aromatic C=C stretching at 1620 and 1570 cm^{-1}, C–O stretching at 1270 and 1180 cm^{-1}, aromatic C=C bending at 840 cm^{-1}, and C–H bending at 770 cm^{-1}. Although the two samples show similar types of functional groups, the relative intensities of the peaks are somewhat different. The aromatic C=C stretching and bending peaks are stronger in S_N than S_A, while the peaks of oxygen-containing groups are more intensified in S_A. These results demonstrate that S_N has the chemical structure of graphitic CNDs, while the main component of S_A is not the same as S_N.

The PLs of S_A, S_N, and the remaining residue after the washouts were collected to confirm the emissive species present in each washout, as shown in Fig. S7 (a–c) (ESI†). The PL spectrum of S_A (Fig. S7(a), ESI†) resembles those of F_Y and F_G. The sharp emission in the blue region corresponds to pyrene monomer emission. Clearly the majority of molecular fluorophores are partitioned to S_A. This is in good agreement with the results of MALDI-TOF, TEM and XRD analyses. The PL spectrum of the S_N (Fig. S7(b), ESI†) appears to be the combination of the molecular fluorophore and the real CNDs. Possibly some molecular fluorophore molecules can be partitioned into S_N together with CNDs since molecular fluorophores also contains hydroxyl groups. The PL spectrum of the washout residue (Fig. S7(c), ESI†) is very similar to that of F_{CND} which mainly contains the CNDs. This suggests that CNDs with very little or no hydroxyl groups remain in the residue without being extracted into the base solution.

Conclusions

This work demonstrates that highly emissive molecular fluorophores are simultaneously produced in the synthesis of CNDs through hydrothermal condensation of substituted PAHs. By using both column chromatography and a simple solvent-driven extraction, molecular fluorophores were successfully separated from CNDs. Through extensive characterization, molecular fluorophores were identified as small hydrophobic derivatives of pyrene and nitropyrene, showing significantly brighter emission than CNDs. We conclude that molecular fluorophores and CNDs are clearly dissimilar in chemical structure and optical properties. This work sheds light on the formation of hydrophobic molecular fluorophores in the

synthesis of PAH-derived CNDs, which is rarely reported in the community. It also highlights the need for rigorous separation and purification steps in the synthesis of not only hydrophilic CNDs but also low-oxygen-content CNDs.

Author contributions

S. W. K., H.-J. S., H. C., B.-S. K., and D. Y. K. participated in conceiving and designing the project. S. W. K., M. S., and H.-J. S. contributed to the synthesis and characterization of carbon dots. N. L. K., N. H. K., C. J. H., and B.-S. K. and D. Y. K. contributed to the separation of carbon dots and molecular fluorophores, and their characterization. F. Y., S.-Y. K., K. Y. H., W.-J. S., and H. C. assisted in idea development and data interpretation. All authors have given approval to the final version of the manuscript.

Conflicts of interest

There are no conflicts to declare.

Acknowledgements

This work was supported by a Samsung GRO award. NHK and BSK appreciate the support from the National Research Foundation of Korea (NRF-2017M3A7B4052802). NK, FY, and DYK are grateful for the support by the NSF through the grant CMMI-1854554.

Notes and references

1 Z. Zhang, J. Zhang, N. Chen and L. Qu, *Energy Environ. Sci.*, 2012, **5**, 8869–8890.
2 X. Du, I. Skachko, A. Barker and E. Y. Andrei, *Nat. Nanotechnol.*, 2008, **3**, 491–495.
3 Y. Yan, J. Gong, J. Chen, Z. Zeng, W. Huang, K. Pu, J. Liu and P. Chen, *Adv. Mater.*, 2019, **31**, e1808283.
4 T. Wang, A. Wang, R. Wang, Z. Liu, Y. Sun, G. Shan, Y. Chen and Y. Liu, *Sci. Rep.*, 2019, **9**, 1–9, DOI: **10.1038/s41598-019-47168-7**.
5 V. Gupta, N. Chaudhary, R. Srivastava, G. D. Sharma, R. Bhardwaj and S. Chand, *J. Am. Chem. Soc.*, 2011, **133**, 9960–9963.
6 W. Kwon, Y. H. Kim, C. L. Lee, M. Lee, H. C. Choi, T. W. Lee and S. W. Rhee, *Nano Lett.*, 2014, **14**, 1306–1311.
7 H. B. Yang, Y. Q. Dong, X. Wang, S. Y. Khoo and B. Liu, *ACS Appl. Mater. Interfaces*, 2014, **6**, 1092–1099.
8 Y. Li, Y. Hu, Y. Zhao, G. Shi, L. Deng, Y. Hou and L. Qu, *Adv. Mater.*, 2011, **23**, 776–780.
9 Z. Zhu, J. Ma, Z. Wang, C. Mu, Z. Fan, L. Du, Y. Bai, L. Fan, H. Yan, D. L. Phillips and S. Yang, *J. Am. Chem. Soc.*, 2014, **136**, 3760–3763.
10 X. T. Zheng, A. Than, A. Ananthanaraya, D. H. Kim and P. Chen, *ACS Nano*, 2013, **7**, 6278–6286.
11 S. Zhu, J. Zhang, C. Qiao, S. Tang, Y. Li, W. Yuan, B. Li, L. Tian, F. Liu, R. Hu, H. Gao, H. Wei, H. Zhang, H. Sun and B. Yang, *Chem. Commun.*, 2011, **47**, 6858–6860.
12 Q. Liu, B. Guo, Z. Rao, B. Zhang and J. R. Gong, *Nano Lett.*, 2013, **13**, 2436–2441.
13 Y. Dong, C. Chen, X. Zheng, L. Gao, Z. Cui, H. Yang, C. Guo, Y. Chi and C. M. Li, *J. Mater. Chem.*, 2012, **22**, 8764–8766.
14 L. Li, G. Wu, G. Yang, J. Peng, J. Zhao and J. J. Zhu, *Nanoscale*, 2013, **5**, 4015–4039.
15 J. Liu, R. Li and B. Yang, *ACS Cent. Sci.*, 2020, **6**, 2179–2195.
16 D. Qu and Z. Sun, *Mater. Chem. Front.*, 2020, **4**, 400–420.
17 F. Yuan, T. Yuan, L. Sui, Z. Wang, Z. Xi, Y. Li, X. Li, L. Fan, Z. A. Tan, A. Chen, M. Jin and S. Yang, *Nat. Commun.*, 2018, **9**, 1–11, DOI: **10.1038/s41467-018-04635-5**.
18 W. Kwon, S. Do, J.-H. Kim, M. Seok Jeong and S.-W. Rhee, *Sci. Rep.*, 2015, **5**, 12604.
19 F. Yuan, Y.-K. Wang, G. Sharma, Y. Dong, X. Zheng, P. Li, A. Johnston, G. Bappi, J. Z. Fan, H. Kung, B. Chen, M. I. Saidaminov, K. Singh, O. Voznyy, O. M. Bakr, Z.-H. Lu and E. H. Sargent, *Nat. Photonics*, 2019, **14**, 171–176.
20 N. Fuyuno, D. Kozawa, Y. Miyauchi, S. Mouri, R. Kitaura, H. Shinohara, T. Yasuda, N. Komatsu and K. Matsuda, *Adv. Opt. Mater.*, 2014, **2**, 983–989.
21 M. Zhao, F. Yang, Y. Xue, D. Xiao and Y. Guo, *ChemPhysChem*, 2014, **15**, 950–957.
22 R. L. Calabro, D.-S. Yang and D. Y. Kim, *ACS Appl. Nano Mater.*, 2019, **2**, 6948–6959.
23 L. Bao, Z. L. Zhang, Z. Q. Tian, L. Zhang, C. Liu, Y. Lin, B. Qi and D. W. Pang, *Adv. Mater.*, 2011, **23**, 5801–5806.
24 L. Wang, S.-J. Zhu, H.-Y. Wang, Y.-F. Wang, Y.-W. Hao, J.-H. Zhang, Q.-D. Chen, Y.-L. Zhang, W. Han, B. Yang and H.-B. Sun, *Adv. Opt. Mater.*, 2013, **1**, 264–271.
25 H. Zheng, Q. Wang, Y. Long, H. Zhang, X. Huang and R. Zhu, *Chem. Commun.*, 2011, **47**, 10650–10652.
26 S. Wang, I. S. Cole, D. Zhao and Q. Li, *Nanoscale*, 2016, **8**, 7449–7458.
27 S. Zhu, J. Shao, Y. Song, X. Zhao, J. Du, L. Wang, H. Wang, K. Zhang, J. Zhang and B. Yang, *Nanoscale*, 2015, **7**, 7927–7933.
28 L. Wang, Y. Wang, T. Xu, H. Liao, C. Yao, Y. Liu, Z. Li, Z. Chen, D. Pan, L. Sun and M. Wu, *Nat. Commun.*, 2014, **5**, 5357.
29 J. B. Essner, J. A. Kist, L. Polo-Parada and G. A. Baker, *Chem. Mater.*, 2018, **30**, 1878–1887.
30 V. Hinterberger, C. Damm, P. Haines, D. M. Guldi and W. Peukert, *Nanoscale*, 2019, **11**, 8464–8474.
31 R. Liu, D. Wu, X. Feng and K. Mullen, *J. Am. Chem. Soc.*, 2011, **133**, 15221–15223.
32 Y. Song, S. Zhu, S. Zhang, Y. Fu, L. Wang, X. Zhao and B. Yang, *J. Mater. Chem. C*, 2015, **3**, 5976–5984.
33 L. Shi, J. H. Yang, H. B. Zeng, Y. M. Chen, S. C. Yang, C. Wu, H. Zeng, O. Yoshihito and Q. Zhang, *Nanoscale*, 2016, **8**, 14374–14378.
34 V. Strauss, H. Wang, S. Delacroix, M. Ledendecker and P. Wessig, *Chem. Sci.*, 2020, **11**, 8256–8266.
35 N. Dhenadhayalan, K.-C. Lin, R. Suresh and P. Ramamurthy, *J. Phys. Chem. C*, 2016, **120**, 1252–1261.

36 T. Lee, S. Won, Y. Park and W. Kwon, *ACS Appl. Nano Mater.*, 2021, **4**, 2462–2469.
37 S. Kaplan, *Org. Magn. Reson.*, 1981, **15**, 197–199.
38 H. S. Rosenkranz, E. C. McCoy, D. R. Sanders, M. Butler, D. K. Kiriazides and R. Mermelstein, *Science*, 1980, **209**, 1039–1043.
39 J. Wu, W. Pisula and K. Mullen, *Chem. Rev.*, 2007, **107**, 718–747.
40 X. Yang, X. Dou, A. Rouhanipour, L. Zhi, H. J. Rader and K. Mullen, *J. Am. Chem. Soc.*, 2008, **130**, 4216–4217.
41 P. G. Ren, D. X. Yan, X. Ji, T. Chen and Z. M. Li, *Nanotechnology*, 2011, **22**, 055705.
42 N. C. Verma, A. Yadav and C. K. Nandi, *Nat. Commun.*, 2019, **10**, 2391.
43 R. Rajendran, S. Sohila, R. Muralidharan, C. Muthamizhchelvan and S. Ponnusamy, *Eur. J. Inorg. Chem.*, 2014, 392–396.
44 M. El Idrissi, S. J. Teat, P. F. Corvini, M. J. Paterson, S. J. Dalgarno and P. Shahgaldian, *Chem. Commun.*, 2017, **53**, 1973–1976.
45 A. Rizzi, P. Cosmina, C. Flego, L. Montanari, R. Seraglia and P. Traldi, *J. Mass Spectrom.*, 2006, **41**, 1232–1241.
46 L. Becker, T. E. Bunch and L. J. Allamandola, *Nature*, 1999, **400**, 227–228.